Dalton Transactions

Accepted Manuscript

ROYAL SOCIETY OF CHEMISTRY

www.rsc.org/dalton

Journal Name

COMMUNICATION

A Kirkendall effect to oxynitride nanotubes towards visible light driven conversion of CO_2 into CH_4†

Received 00th January 20xx,
Accepted 00th January 20xx

DOI: 10.1039/x0xx00000x

www.rsc.org/

P. Zhou,[a] H. L. Gao,[b] S. C. Yan,*[bc] and Z. G. Zou,[abc]

Functional hollow nanomaterials are of great interests due to their unique physical-chemistry properties. Oxynitrides photocatalyst was a kind of promising materials for solar energy conversion. However, nanoscale design of hollow oxynitrides was difficult to achieve due to the thermal instability of oxide precursors under high temperature. Here, single crystal zinc gallium oxynitride nanotubes were successfully synthesized via a Kirkendall effect with ZnO nanorods and Ga_2O_3 nanosheet as precursors, which can be attributed to the high diffusion rate of ZnO and high melting point of oxynitride. Enhanced photocatalytic performance in CO_2 reduction was achieved over as-prepared ZnGaNO nanotubes, due to higher specific surface area and less recombination of photogenerated carriers. These results are expected to provide new guidance for the design and preparation of high efficient nano-scaled oxynitride photocatalysts.

Introduction

Functional materials with hollow nanostructures have raised considerable attentions, owing to their unique physical and chemical properties that achieve extensive applications in many fields such as the gas sensing,[1] optoelectronics,[2] field emission,[3] drug delivery,[4, 5] luminescence,[6, 7] and photocatalysis.[8, 9] Many methods have been developed for the synthesis of hollow nanostructures, such as sacrificial templates,[10] anodization,[11, 12] self-organization[13, 14] and Kirkendall effect.[15, 16]

Oxynitrides, which usually have suitable band gap that can absorb visible light, are promising photocatalytic materials for solar energy conversion.[17-21] A popular route to the synthesis of oxynitrides is to directly nitride the corresponding oxide precursors at high temperatures (800–1000°C).[22, 23] This means that it is difficult to achieve the nanoscale design of oxynitrides catalyst due to the thermal instability of oxide precursors under high temperature. Recently, we have developed a molten salt ion-exchange method to prepare ZnGaNO nanorods, which exhibited the improved performance in CO_2 reduction thanks to the high specific surface area and less crystal defects.[24]

Kirkendall effect, a classical phenomenon in metallurgy, has also been found to be an efficient route to obtain the porous materials, where formation of pores resulted from the different diffusion rates between two components in diffusion couple.[25] Hollow nanomaterials synthesized *via* Kirkendall effect has been achieved in binary and ternary materials, such as ZnO hollow nanoparticles,[26] ZnS hollow nanospheres,[27] and $ZnAl_2O_4$ crystalline nanotubes.[15] It was found that ZnO is an excellent core material in forming voids due to its relatively high diffusion rate. Here, we show that the hexagonal ZnGaNO oxynitride nanotubes can be successfully fabricated with hexagonal zinc oxide (ZnO) nanorods as a starting material via a Kirkendall effect by ZnO diffusing into the GaN, exhibiting the high performance in photoreduction of carbon dioxide into methane.

Experimental

Sample preparation

The ZnO nanorod was synthesized using $Zn(NO_3)_2 \cdot 6H_2O$ and ammonia hydroxide as precursors. Typically, 2.5g $Zn(NO_3)_2 \cdot 6H_2O$ and 1.0g ammonia hydroxide was added into 100ml deionized water, and put in a water bath at 90°C for 4h.

The Ga_2O_3 nanosheet was synthesized by a hydrothermal ion-exchange reaction followed by a dehydration heat treatment. First, 1.3821g K_2CO_3 and 1.8744g commercial Ga_2O_3 was evenly mixed, and calcined at 900°C for 16h to get pure $KGaO_2$. Then, 1.1264g $KGaO_2$ was added into 150ml water to get a clear solution, followed by adding 0.48g acetic acid slowly. And the solution was stirred in ambient condition for half an hour, and then put into a water bath at 80°C for 3h to get

[a] National Laboratory of Solid State Microstructures, Eco-Materials and Renewable Energy Research Center (ERERC), School of Physics, Nanjing University, No. 22, Hankou Road, Nanjing, Jiangsu 210093, PR China.
[b] Collaborative Innovation Center of Advanced Microstructures, College of Engineering and Applied Sciences, Nanjing University, No. 22, Hankou Road, Nanjing, Jiangsu 210093, PR China. E-mail: yscfei@nju.edu.cn.
[c] Jiangsu Key Laboratory for Nano Technology, Nanjing 210093, P.R.China.
† Electronic Supplementary Information (ESI) available: EDX analysis and SEM images of ZGNO-SSR and ZnGaNO nanoflowers. See DOI: 10.1039/x0xx00000x

GaOOH. Then, the as-prepared GaOOH was calcined at 800°C for 2h with 50sccm oxygen flow to get β-Ga_2O_3 nanosheet.
The ZnGaNO nanotube was synthesized by nitriding the mixture of as-prepared ZnO nanorod and Ga_2O_3 nanosheet at 800°C for 5h with 500sccm NH_3 flow, followed by loading 0.5wt% Pt as cocatalyst by impregnation method.

The ZnGaNO-SSR was synthesized by nitriding the mixture of ZnO and Ga_2O_3 at 850°C for 15h, followed by loading 0.5wt% Pt as cocatalyst by impregnation method.

Sample characterization

The crystal phase of the derived sample was determined by an X-ray diffractometer (XRD, Rigaku Ultima III, Japan) operated at 20kV and 40mA with Cu-Kα radiation. Diffused reflectance spectrum was scanned by a UV-vis spectrophotometer (UV-2500, Shimadzu Co., Japan) and transformed into absorption spectrum with Kubelka–Munk relationship. The specific surface area was measured on nitrogen adsorption at -196°C by an automatic surface area analyzer (Micromeritics Tristar-3000, USA) after the samples had been dehydrated in the flow of N_2 at 150°C for 3h. The surface morphology was characterized by scanning electron microscope (SEM, FEI Nova Nano SEM 230, USA). TEM images and selected area electron diffraction patterns (SAED) was obtained by employing a transmission electron microscope (TEM, FEI Tecnai G2 F30 S-Twin, USA) operated at 200 kV. The transmission infrared spectra were measured by an Infrared Spectroscopy (FT-IR spectrometer, NEXUS870, Nicolet, USA) at ambient condition.

Photocatalytic evaluation

The photocatalytic CO_2 reaction was carried out in a glass reactor with an area of 4.2 cm^2. The light source was a 300W Xenon arc lamp from PerfectLight Company, and to get a visible irradiation, a 420nm filter was employed. The volume of the reaction chamber was about 230ml. Before the reaction, the chamber was evacuated several times and then high purity CO_2 gas was introduced into the reaction chamber to achieve ambient pressure. 0.4ml deionized water was injected into the chamber as reactant. During the reaction, 1ml gas was extracted by a sampling needle from the chamber at given intervals for subsequent CH_4 concentration analysis with gas chromatography (GC-2014, Shimadzu Corp., Japan).

Results and discussion

To synthesize the ZnGaNO nanotubes, a mixture of ZnO nanorods and Ga_2O_3 nanoplates was employed as raw materials. The ZnO nanorods were first synthesized by a water bath heating of $Zn(CH_3COO)_2$ and ammonia, and the Ga_2O_3 nanoplates were synthesized by a hydrothermal ion-exchange reaction of $KGaO_2$ and CH_3COOH and followed by dehydroxylation treatment (see Experiment section in ESI†). Then, the mixture of ZnO nanorods and Ga_2O_3 nanoplates was nitrided at 750°C for 5h under 250mL min^{-1} flowing NH_3 to get the ZnGaNO nanotubes. The phase compositions for the precursors and products were confirmed by XRD patterns, as shown in Fig. 1a. We can see that both of the precursors, ZnO

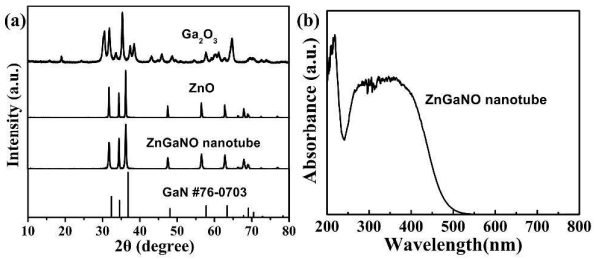

Fig. 1 (a) XRD patterns of precursors Ga_2O_3, ZnO ZnGaNO and GaN (JCPDS card no. 76-0703). (b) UV-Vis absorption spectrum of as-prepared ZnGaNO solid solution.

and Ga_2O_3, were well crystallized with no impurity phase. XRD peaks for the mixture of ZnO and Ga_2O_3 after nitriding located between those of ZnO and GaN, indicating that the nitriding product is a solid solution of ZnO and GaN, as demonstrated in previous reports.[28] In addition, the UV-Vis absorption spectrum shown in Fig. 1b is another evidence to the formation of ZnGaNO solid solution. The band gap of the as-prepared ZnGaNO solid solution can be determined to be ca. 2.58eV, based on an absorption edge of ca. 480nm, which is lower than the band gap of either ZnO (3.2eV) or GaN (3.4eV), further confirming that the nitriding product ZnGaNO is a solid solution of GaN and ZnO. As a solid solution, the bandgap has been shown to depend strongly on the zinc or oxygen concentration due to the influence on structural and electronic properties.[29] Energy dispersive X-ray spectrum (EDX) analysis showed that the Zn:Ga atom ratio of the as-prepared ZnGaNO solid solution was almost 1:2, which was in accordance with the band gap of 2.58eV according to the empirical formula given by Muckerman's group.[29]

The morphologies of these as-prepared products were characterized by SEM and TEM, as shown in Fig.2. It reveals that the precursors ZnO and Ga_2O_3 are hexagonal single-crystal nanorods (Fig. 2a) and diamond single-crystal nanoplates (Fig. 2b), respectively. The length of the ZnO nanorods is about 600-900nm, and the diameter is about 200nm. As shown in Fig.2c and 2d, ZnGaNO nanotubes were well synthesized after nitriding the mixture of ZnO nanorods and Ga_2O_3 nanoplates. The length of the nanotubes is about 600~900nm, and the diameter is about 200nm with about 40nm thick walls. The cross-section image in Fig. 2d and TEM image in Fig. 2e also

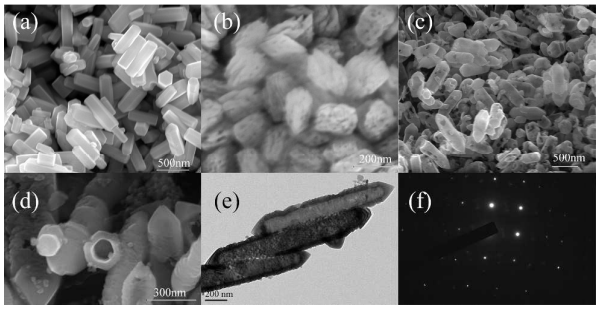

Fig. 2 SEM images of ZnO nanorods (a), Ga_2O_3 nanoplates (b), ZnGaNO nanotubes (c) and cross section of ZnGaNO nanotubes (d), TEM image of ZnGaNO nanotubes (e), SAED patterns of ZnGaNO nanotubes.

evidenced the hollow structures of derived ZnGaNO nanotubes. The selected area electron diffraction (SAED) pattern was presented in Fig. 2f, which clearly demonstrated that the ZnGaNO nanotubes are single crystals.

As can be seen from Fig. 2, the length and diameter of ZnGaNO nanotube and ZnO nanorod are almost the same. This indicates that the size and shape of ZnGaNO nanotube could be remained from the precursor ZnO nanorod. In the reaction, atoms would diffuse across the contact interface in different diffusion rates, and defects may form and accumulate into pores on the side with higher diffusion rate. This indicated that a Kirkendall effect may occur. To synthesize porous materials via Kirkendall effect, materials with high diffusion rates as templates were required. In our precursors, ZnO is a high-diffusion material, which has been applied in synthesizing binary and ternary hollow structures by Kirkendall effect, as reported in previous literature.[15, 26, 27] It is also observed in our experiment that ZnO could be a suitable template to facilitate the formation of quaternary hollow nanotubes. Based on these knowledges, a growing process was proposed, as illustrated in Fig. 3. First, the Ga_2O_3 nanoparticles and NH_3 react on the surface of hexagonal ZnO nanorod. By mechanically mixing, rough contact interfaces were formed between ZnO nanorods and Ga_2O_3 nanoplates. Under high temperature calcination, atoms would diffuse across the contact interfaces, that is the N and Ga atoms would gradually migrate inward and the Zn and O atoms migrate outward. Nanoscale Ga_2O_3 nanoplates would make a better contact interfaces and better interdiffusion. With the diffusion going on, a ZnGaNO layer was formed on the surface of ZnO nanorod. At the same time, the outer layer Ga_2O_3 would be nitride into GaN. As ZnO and GaN have similar wurtzite structure, the wurtzite lattice may facilitate the interdiffusion as atoms would diffuse along the wurtzite structures. During the diffusion process, vacancies appear in the center of ZnO nanorod and gradually accumulate into holes due to the high outward diffusion velocities of Zn and O atoms. With diffusion process to proceed, the holes along the center of ZnO nanorod become larger and larger, and finally to form a nanotube with a skeleton of hexagonal ZnO nanorod. Though the skeletons of the precursors were usually collapsed at high temperatures, the skeletons of ZnO nanorods were perfectly preserved in the oxynitride product, which may credit to the high melting points of oxynitride.[30] Under high temperature calcination, the oxynitride skeleton that has been formed would not be melted, leading to the reservation of the hexagonal skeleton and formation of the final product ZnGaNO nanotubes.

Furthermore, the sizes of the ZnGaNO nanotubes are controllable. As can be seen from the above results, the morphology of ZnGaNO nanotube was mainly a copy of the

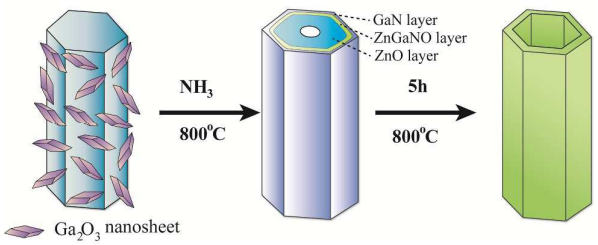

Fig. 3 The schematic graph to show the forming process of ZnGaNO nanotube via a Kirkendall effect

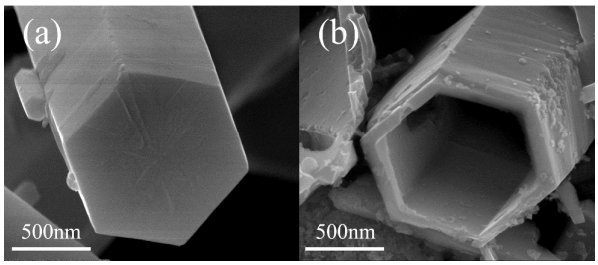

Fig. 4 SEM images of ZnO rods (a) and ZnGaNO tubes (b)

profile of the hexagonal ZnO nanorods. While with different sizes of the ZnO nanorods precursors, different sizes of the ZnGaNO nanotubes can be obtained. In Fig. 4a, we synthesized larger size of ZnO rods by hydrothermal method. With larger ZnO rods as templates, larger ZnGaNO tubes were obtained, as shown in Fig. 4b. Also, based on the knowledge of the proposed growing process, it is interesting to find that using the different shapes of the precursor ZnO will lead to different morphologies of ZnGaNO products. Indeed, ZnGaNO nanoflowers were successfully synthesized via Kirkendall effect by using the ZnO nanoflowers as precursor, as illustrated in Fig. S2. This indicated that such a synthetic method can be widely applied to fabricate the various shapes of ZnGaNO oxynitrides.

The photocatalytic performance of the as-prepared ZnGaNO nanotubes (denoted as ZGNO-nanotube) was conducted by CO_2 photoreduction. Fig. 5a shows that CO_2 can be photoreduced into CH_4 over ZnGaNO nanotubes loaded with 0.5wt% Pt as co-catalyst in the presence of water vapor under visible light irradiation (420nm filter). For comparison, the photoreduction performances of ZnGaNO nanoparticles synthesized by the solid state reaction of ZnO and Ga_2O_3 at 850°C under flowing NH_3 for 15h (denoted as ZGNO-SSR), ZnGaNO nanorods synthesized by molten salt ion-exchange method [31] and ZnGaNO tubes synthesized with ZnO rods were also examined. The CO_2 photoreduction experiment showed that the methane evolution had a relatively good linear relationship with increased irradiation time. As calculated from the slope of the gas evolution curves, the production rate of methane was about 0.072μmol$g^{-1}h^{-1}$ for ZGNO-nanotube, which was about 2 times

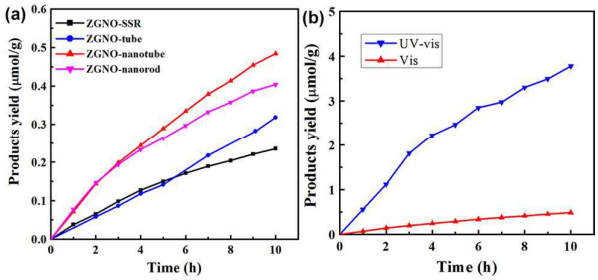

Fig. 5 The time course evolution of methane yields by CO_2 photoreduction under visible light irradiation over ZGNO-nanotube, ZGNO-SSR, ZGNO-tube and ZGNO-nanorod (a) and a comparison of full-arc and visible light irradiation over ZGNO-nanotube (b).

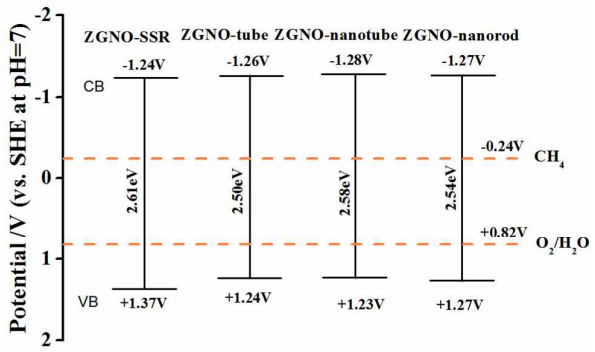

Fig. 6 The band structures of ZGNO-SSR, ZGNO-tube, ZGNO-nanotube and ZGNO-nanorod at pH=7.

higher than 0.033μmolg^{-1}h^{-1} for ZGNO-SSR. The ZGNO-nanorod has almost the same activity as ZGNO-nanotube in the first four hours, and then gradually decreased. Under full-arc light irradiation (Fig.5b), the CH_4 production rate over ZnGaNO nanotubes was about 0.60μmolg^{-1}h^{-1}, about 8 times higher than that under visible light irradiation, probably due to more light absorption and less bulk recombination from shorter penetration depth of ultraviolet light.

The valance band maximum position of ZnGaNO solid solutions was determined by XPS (Fig. S5). As illustrated in Fig. 6, the maximum valance bands of ZGNO-SSR, ZGNO-tube, ZGNO-nanotube and ZGNO-nanorod are at +1.37V, +1.24V, +1.23V and +1.27V, respectively. The minimum conduction band position can be obtained by the formula: $E_g=E_{VBM}-E_{CBM}$, where E_g is the band gap, E_{VBM} is the valence band maximum and E_{CBM} is the conduction band minimum. The band gaps of ZGNO-SSR, ZGNO-tube, ZGNO-nanotube and ZGNO-nanorod are obtained from the UV-Vis absorption spectra to be 2.61eV, 2.50eV, 2.58eV and 2.54eV, respectively (Fig. S4). Thus, the minimum conduction band position of ZGNO-SSR, ZGNO-tube, ZGNO-nanotube and ZGNO-nanorod are at -1.24V, -1.26V, -1.28V and -1.27V respectively, as shown in Fig. 6. The conduction bands for these samples used in this study are higher than -0.24V, and valance band is lower than +0.82V, indicating that the band structure of ZnGaNO solid solution is able to oxide water and reduce CO_2 into CH_4.

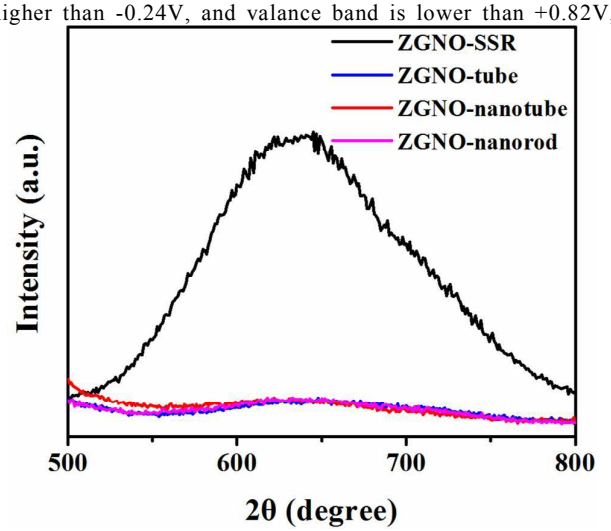

Fig. 7 The photoluminescence spectra of ZGNO-SSR and ZGNO-nanotube. Excitation: 410nm.

One possible reason for the improvement of the CO_2 photocatalytic reduction performance of ZnGaNO was the increased specific surface area. The nitrogen adsorption–desorption measurement indicated that the specific surface area of the ZGNO-nanotube was 12.1m^{2}g^{-1}, almost twice as much as 5.9m^{2}g^{-1} for ZGNO-SSR, and higher than 9.7 m^{2}g^{-1} for ZGNO-tube. Larger surface area would provide more active sites and adsorption areas, leading to a higher photoreduction activity. It is worth pointing out that the ZnGaNO nanorods with larger specific surface area of 18.7m^{2}g^{-1} exhibited the same activity as ZnGaNO nanotubes (12.1m^{2}g^{-1}), probably due to the nanotubes having increasing light utility by scattering and shorting carriers diffusion distance in the tube wall. After 4h light irradiation (Fig.5a), the activity of ZnGaNO nanorods decreased. The decrease in activity probably originated from the photocorrosion due to long carriers diffusion distance from the inner to the surface of nanorods.

In addition, the crystal structure could be another reason for the improvement of the photocatalytic performance. It was reported that materials with wurtzite structure such as ZnO and GaN would have spontaneous polarization along the *c*-axis.[32, 33] In our case, as a solid solution of ZnO and GaN, ZnGaNO nanotubes, which were a single crystal with a preponderant growth along *c*-axis, share the same wurtzite structure, meaning that ZnGaNO also has spontaneous polarization effect and forms a uniform polarized electric field in the single crystal. Under the polarized electric field, electrons and holes would transfer in the opposite direction, thus can be effectively separated, leading to less recombination. Additionally, electron and hole transportation paths would form separately in the direction perpendicular to the c-axis, decreasing the recombination probability. In addition, the thin shell of the ZnGaNO nanotubes made the photo-generated carriers easier to transport to the surfaces instead of recombination. To compare the carrier recombination of those samples, photoluminescence (PL) analysis were conducted. The photoluminescence spectrum in Fig. 7 demonstrated that the ZGNO-SSR had a high photoluminescence peak at 640nm, which can be attributed to the strong recombination of photogenerated carriers at the crystal defects formed during the high-temperature calcination.[34-36] In comparison, ZGNO-tube, ZGNO-nanotube and ZGNO-nanorod showed quite weaken photoluminescence intensities, indicating the those samples had less radiative recombination of photogenerated carriers, leading to higher photocatalytic CO_2 reduction performance.

Conclusions

In summary, we demonstrated that the quaternary oxynitride ZnGaNO nanotubes can be successfully fabricated by a Kirkendall effect. The enhanced photocatalytic performance in CO_2 reduction was achieved over as-prepared ZnGaNO nanotubes due to its higher specific surface area and less recombination of photogenerated carriers. The new synthetic strategy may provide a new guidance for the design and preparation of efficient nano-scaled oxynitride photocatalysts.

Acknowledgements

This work was supported primarily by the National Basic Research Program of China (2013CB632404), and the National Natural Science Foundation of China (51572121).

References

1. M. S. Arnold, P. Avouris, Z. W. Pan and Z. L. Wang, *J Phys Chem B*, 2003, 107, 659-663.
2. Y. N. Xia, P. D. Yang, Y. G. Sun, Y. Y. Wu, B. Mayers, B. Gates, Y. D. Yin, F. Kim and Y. Q. Yan, *Adv Mater*, 2003, 15, 353-389.
3. C. H. Liu, J. A. Zapien, Y. Yao, X. M. Meng, C. S. Lee, S. S. Fan, Y. Lifshitz and S. T. Lee, *Adv Mater*, 2003, 15, 838-839.
4. A. Bianco, K. Kostarelos and M. Prato, *Curr Opin Chem Biol*, 2005, 9, 674-679.
5. S. S. Li, H. He, Q. C. Jiao and P. H. Chuong, *Prog Chem*, 2008, 20, 1798-1803.
6. J. E. Riggs, Z. X. Guo, D. L. Carroll and Y. P. Sun, *J Am Chem Soc*, 2000, 122, 5879-5880.
7. J. M. Bonard, T. Stockli, F. Maier, W. A. de Heer, A. Chatelain, J. P. Salvetat and L. Forro, *Phys Rev Lett*, 1998, 81, 1441-1444.
8. I. Paramasivam, H. Jha, N. Liu and P. Schmuki, *Small*, 2012, 8, 3073-3103.
9. M. Y. Wang, J. Ioccozia, L. Sun, C. J. Lin and Z. Q. Lin, *Energ Environ Sci*, 2014, 7, 2182-2202.
10. G. Che, B. B. Lakshmi, C. R. Martin, E. R. Fisher and R. S. Ruoff, *Chem Mater*, 1998, 10, 260-267.
11. J. M. Macak, H. Tsuchiya and P. Schmuki, *Angew Chem Int Edit*, 2005, 44, 2100-2102.
12. H. E. Prakasam, K. Shankar, M. Paulose, O. K. Varghese and C. A. Grimes, *J Phys Chem C*, 2007, 111, 7235-7241.
13. Q. W. Li, Y. T. Zhu, I. A. Kinloch and A. H. Windle, *J Phys Chem B*, 2006, 110, 13926-13930.
14. O. A. Louchev and Y. Sato, *Appl Phys Lett*, 1999, 74, 194-196.
15. H. J. Fan, M. Knez, R. Scholz, K. Nielsch, E. Pippel, D. Hesse, M. Zacharias and U. Gosele, *Nat Mater*, 2006, 5, 627-631.
16. F. Aldinger, *Acta Metall Mater*, 1974, 22, 923-928.
17. K. Ueda, T. Minegishi, J. Clune, M. Nakabayashi, T. Hisatomi, H. Nishiyama, M. Katayama, N. Shibata, J. Kubota, T. Yamada and K. Domen, *J Am Chem Soc*, 2015, 137, 2227-2230.
18. M. Jansen and H. P. Letschert, *Nature*, 2000, 404, 980-982.
19. L. Zhang, Y. Song, J. Y. Feng, T. Fang, Y. J. Zhong, Z. S. Li and Z. G. Zou, *Int J Hydrogen Energ*, 2014, 39, 7697-7704.
20. M. Higashi, K. Domen and R. Abe, *J Am Chem Soc*, 2013, 135, 10238-10241.
21. T. Ohno, L. Bai, T. Hisatomi, K. Maeda and K. Domen, *J Am Chem Soc*, 2012, 134, 8254-8259.
22. M. Y. Liu, W. S. You, Z. B. Lei, G. H. Zhou, J. J. Yang, G. P. Wu, G. J. Ma, G. Y. Luan, T. Takata, M. Hara, K. Domen and L. Can, *Chem Commun*, 2004, 2192-2193.
23. R. Aguiar, A. Kalytta, A. Reller, A. Weidenkaff and S. G. Ebbinghaus, *J Mater Chem*, 2008, 18, 4260-4265.
24. P. Zhou, S. C. Yan and Z. G. Zou, *Crystengcomm*, 2015, 17, 992-995.
25. H. J. Fan, U. Gosele and M. Zacharias, *Small*, 2007, 3, 1660-1671.
26. R. Nakamura, J. G. Lee, D. Tokozakura, H. Mori and H. Nakajima, *Mater Lett*, 2007, 61, 1060-1063.
27. H. F. Shao, X. F. Qian and Z. K. Zhu, *J Solid State Chem*, 2005, 178, 3522-3528.
28. H. Y. Chen, L. P. Wang, J. M. Bai, J. C. Hanson, J. B. Warren, J. T. Muckerman, E. Fujita and J. A. Rodriguez, *J Phys Chem C*, 2010, 114, 1809-1814.
29. L. L. Jensen, J. T. Muckerman and M. D. Newton, *J Phys Chem C*, 2008, 112, 3439-3446.
30. B. Mazumder and A. L. Hector, *J Mater Chem*, 2009, 19, 4673-4686.
31. K. Teramura, K. Maeda, T. Saito, T. Takata, N. Saito, Y. Inoue and K. Domen, *J Phys Chem B*, 2005, 109, 21915-21921.
32. F. Bernardini, V. Fiorentini and D. Vanderbilt, *Phys Rev B*, 1997, 56, 10024-10027.
33. Z. L. Wang, *Annu Rev Phys Chem*, 2004, 55, 159-196.
34. Y. C. Lee, T. Y. Lin, C. W. Wu, H. S. Teng, C. C. Hu, S. Y. Hu and M. D. Yang, *J Appl Phys*, 2011, 109, 073506.
35. D. Li, Y. H. Leung, A. B. Djurisic, Z. T. Liu, M. H. Xie, S. L. Shi, S. J. Xu and W. K. Chan, *Appl Phys Lett*, 2004, 85, 1601-1603.
36. A. B. Djurisic, Y. H. Leung, K. H. Tam, L. Ding, W. K. Ge, H. Y. Chen and S. Gwo, *Appl Phys Lett*, 2006, 88, 103107.